Progress in Natural Science: Materials International 2013;23(5):475–480

Chinese Materials Research Society

Progress in Natural Science: Materials International

www.elsevier.com/locate/pnsmi
www.sciencedirect.com

ORIGINAL RESEARCH

Differences between amorphous indium oxide thin films

D. Bruce Buchholz, Li Zeng, Michael J. Bedzyk, Robert P.H. Chang*

Department of Materials Science and Engineering, Northwestern University, Evanston, IL 60208, USA

Received 14 February 2013; accepted 27 May 2013
Available online 14 October 2013

KEYWORDS

Transparent conducting oxide;
Semiconductor;
Oxide;
Amorphous;
Deposition temperature

Abstract A series of ~60 nm thick indium oxide thin-films, all amorphous as determined by x-ray diffraction, were found to have physical and electrical properties that depended on the temperature of deposition. The carrier mobility and film conductivity decreased with decreasing deposition temperature; the best electrical properties of high mobility and conductivity were observed at a deposition temperature just below the temperature at which crystalline films formed. The density of the film also decreased with deposition temperature from 7.2 g/cm^3 at +50 °C to 5.3 g/cm^3 at −100 °C.

1. Introduction

Transparent conducting oxides (TCOs) have an established record as important materials for photovoltaic devices and optoelectronic applications [1–3]. Transparent oxide semiconductors (TOSs), are currently being explored as thin film transistor (TFT) materials, an enabling technology for the next generation of computing, communication and identification devices [2,4]. Initially, the technological application of TCOs and TOSs employed these materials in their crystalline form. There is, however, an increasing shift towards the use of these materials in their amorphous form. In 2010 an estimated 30–40% of all flat panel displays employed an amorphous TCO material [5].

Amorphous TCOs and TOSs (a-TCOs and a-TOSs) have several advantages over their crystalline counterparts. In general, amorphous materials are deposited at lower temperatures [6] which tends to simplify the deposition process and expands the number of substrates the material can be deposited on, such as plastics. Amorphous materials, because they lack grain boundaries and are isotropic, tend to etch more uniformly [7–9], have lower surface roughness [10,11], and can be deposited uniformly over large areas [8,12]. Some amorphous materials can also be less prone to fracture, hence more pliable, lending themselves to the possibility of flexible electronics [8,13]. These advantages are realized without a significant loss to the seminal properties of conductivity and transparency for optimized amorphous materials [14].

The electrical and optical properties of crystalline TCOs and TOSs (c-TCOs and c-TOSs) are strongly influenced by the oxygen content of the film [15]; the same is true for a-TCOs and a-TOSs [16]. For c-TCOs and c-TOSs their properties are also affected by factors related to the crystal structure such as grain size [17] and crystallographic direction [18]. For a-TCOs and a-TOSs it is tempting to

*Correspondence to: Department of Materials Science and Engineering Northwestern University 2220 Campus Drive, Cook Hall Room 2013 Evanston, IL 60208 USA Tel.: +1 847 491 3598; fax: +1 847 491 4181.
E-mail address: r-chang@northwestern.edu (R.P.H. Chang).

Peer review under responsibility of Chinese Materials Research Society.

ELSEVIER Production and hosting by Elsevier

1002-0071 © 2013 Chinese Materials Research Society. Production and hosting by Elsevier B.V. All rights reserved.
http://dx.doi.org/10.1016/j.pnsc.2013.08.004

assume a single structure and, therefore, that processing induced changes to the material's performance are due to factors other than a change in structure; that for a given material system all amorphous materials would have the same "non-structure". This, however, does not appear to be the case. There are both theoretical and experimental indications that differences exist between amorphous materials of the same material system beyond those caused by differences in oxygen content.

Although pure indium oxide is rarely used in technological applications it is the progenitor of many TCO and TOS systems. Tin, zinc, gallium, as well as other elements, are added to indium oxide to produce technologically useful materials [8,19,20]. Pure indium oxide (IO), however, has an advantage over doped systems as it removes the ambiguity introduced by dopants in comparing experimental studies. Experimentally, the mobility of amorphous IO (a-IO) ranges from 10 $cm^2/V \bullet s$ to 51 $cm^2/V \bullet s$ [21,22]. Although differences in carrier concentration, and hence density of ionized donor centers, can effect mobility [23], the carrier concentrations reported with the above cited mobilities were 2×10^{20} cm^{-3} and 4×10^{20} cm^{-3}, respectively. The carrier concentrations are in the range where ionized donor centers are expected to dominate scattering [24], but with the trend opposite to that expected if the change in mobility were an effect of ionized donor centers. A second difference between the two amorphous materials must exist to explain this range in carrier mobility [25]. In a theoretical study, Rosen et al. [26], varied the cooling time used in molecular dynamics liquid-quench simulations of a-IO. They found that the resulting structures increased in energy (decreased in stability) as the quench time was decreased. They also reported a decrease in both oxygen-indium and indium-indium coordination as quench time decreased (with the exception of the simulation for an instantaneous quench). Although not monotonically increasing as quench time decreased, there was also a general trend towards a larger pseudo lattice constant, *a*, with decreasing quench time, hence a less-dense structure.

The simulations used to generate the model amorphous-structures, used by Rosin and others, typically involve heating the crystalline form of the material to high temperature to randomize the atomic arrangement followed by a rapid-quench to freeze the atomic arrangement in place. Materials grown by pulsed laser deposition (PLD) undergo just such a process. A small spot on a polycrystalline target made of the material to be deposited is rapidly heated by a laser pulse to ablation (2000–3000 K) and then the plume of ablated material rapidly cooled at the substrate. In the study by Rosin, the rate of quenching had an effect on the resulting structure. The analogical variable in a PLD experiment would be the substrate temperature. For 60 nm thick films grown by PLD, indium oxide is x-ray diffraction amorphous up to a deposition temperature of +50 °C. In this study we look at the physical and electrical differences in x-ray diffraction amorphous indium oxide (henceforth simply referred to as a-IO) as a function of deposition temperature for films deposited between −100 °C and +50 °C. Films grown at +75 °C (the temperature at which evidence of crystallinity is first observed) and +400 °C (a completely crystalline film) are also included for comparison.

2. Materials and methods

2.1. Film growth

Indium oxide thin-films, ~60 nm thick, were grown by pulsed-laser deposition (PLD) from a dense hot-pressed indium oxide target (25 mm diameter). PLD was accomplished with a 248 nm KrF excimer laser with a 25 ns pulse duration and operated at 2 Hz. The 200 mJ/pulse beam was focused onto a 1 mm × 2 mm spot size. The target was rotated at 5-rpm about its axis to prevent localized heating. The target-substrate separation was fixed at 10 cm. The films were grown on fused-silica substrates in an O_2 ambient of 8 mTorr. The substrates were attached to the substrate holder with silver paint. For films grown above room temperature a resistively heated substrate-holder was used; for films grown below room temperature a liquid nitrogen cooled substrate-holder was used.

2.2. Film analysis

Sheet resistance (R_s:Ω/□), carrier type, area carrier-concentration (n_a: 1/cm^2), and carrier mobility (μ_H:$cm^2/V \bullet s$) were measured with a Ecopia 3000 Hall measurement system on samples in the van der Pauw geometry. Carrier density (n: 1/cm^3) and resistivity (ρ:Ω• cm) were calculated by dividing the area carrier-concentration and sheet resistance, respectively, by the film thickness. Film thickness (d:nm) was measured using a spectral reflectometer (Filmetrics F20) and were shown to range from 50 to 65 nm. X-ray reflectivity (XRR) was performed using an 18 kW Rigaku ATX-G diffractometer. Cu*K*α radiation ($\lambda = 1.54$ Å) was conditioned by a parabolic multilayer mirror and collimated to produce a 0.1 mm (vertical) by 5 mm (horizontal) beam with incident flux of $\sim 2 \times 10^8$ photons/s. The XRR data was fitted to a two-layer model (film and interfacial layer) calculated by applying Abeles matrix method used in the Motofit package [27] to obtain the thickness, electron density (convertible to mass density given the film composition), and interfacial roughness of each layer. Grazing incidence x-ray diffraction (GIXRD) was performed with the same instrument at a beam incident angle of 0.46°. Film composition was measured by x-ray Photon Spectroscopy (XPS) using a Thermo Scientific ESCALAB 250Xi using a Al Kα source and a take-off angle of 90°. An argon ion source was used to clean carbon from the surface prior to analysis. The flood gun was used on all analysis although it was only needed on the more insulating samples to maintain charge neutrality.

3. Results and discussion

3.1. Effect of deposition temperature on crystallinity

For many thin-film material systems, the transition between amorphous and crystalline can be accomplished by changing the temperature of deposition; the crystalline phase being favored by higher deposition temperatures [28]. Such is the case for IO deposited on fused quartz by PLD. Fig. 1 is the GIXRD spectra of IO films ~60 nm thick. Films grown at temperatures of +50 °C and below are all x-ray diffraction amorphous. The first sign of crystallinity is observed at +75 °C where the c-IO/a-IO ratio, as determined by the area of the crystalline XRD peaks and the area of the "amorphous hump", is 6/94; a crystalline film deposited at 400 °C is included for comparison. The GIXRD spectra for the crystalline film is typical of that observed for polycrystalline bixbyite In_2O_3; the lattice constant, as determine from the locations of the peaks indexed in Fig. 1, is 10.09 Å, slightly less than the value of 10.12 Å frequently quoted for bulk In_2O_3 [29].

3.2. Effect of deposition temperature on density

Although the films deposited between −100 °C and +50 °C are all diffraction amorphous, both their physical and electrical properties

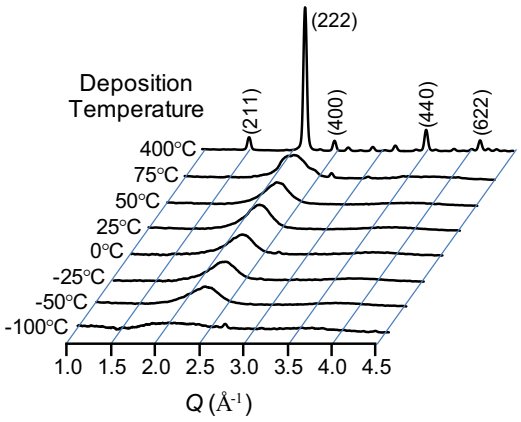

Fig. 1 GIXRD spectra of indium oxide films, ~60 nm thick, as a function of deposition temperature.

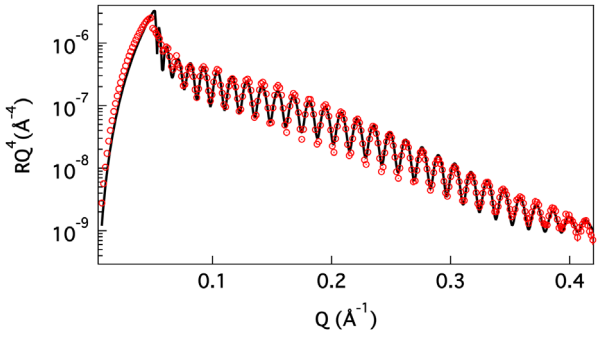

Fig. 2 X-ray reflectivity data (red circles) and the best-fit value (solid black lines) for the indium oxides film grown by PLD at a deposition temperature of 0 °C.

are dependent on deposition temperature. For a given material such as indium oxide, mass density has a linear relation to electron density provided stoichiometry is fixed. Hence, x-ray reflectivity (XRR), a technique sensitive to the electron density profile of the thin films is used to characterize mass density. The reflected photons are collected under the $\Theta/2\Theta$ condition, which keeps the momentum transfer, $Q=4\pi \sin(2\Theta/2)/\lambda$, normal to the surface of the film. Therefore, the reflectivity can be expressed as a function of momentum transfer. The XRR data is fitted to a two-layer model (film and interfacial layer with RMS roughness) calculated by applying Abeles matrix method used in the Motofit package [27] to obtain the thickness and electron density of each layer, as well as interfacial roughness between each layer. Fig. 2 is a typical XRR spectrum and best-fit result performed over a Q range of 0.08–0.4 $Å^{-1}$.

The electron density of the films, as measured by XRR, decreases from a value of 1.89 $Å^{-3}$ at +50 °C, the same as for bulk c-IO, to 1.42 $Å^{-3}$ at −100 °C, a difference of ~30%, Fig. 3. There are two possible origins for the change in density; a change in structure or a change in composition. XPS was used to compare the composition of the films; all the films had the same In/O ratio within ±5% with no observable tend with respect to deposition temperature. The right hand axis of fig. 3 is the mass density assuming a stoichiometry of In_2O_3; again this is a difference of ~30% between +50 °C (7.17 g/cm^3) and −100 °C (5.37 g/cm^3). This difference is large but comparable to that observed in other

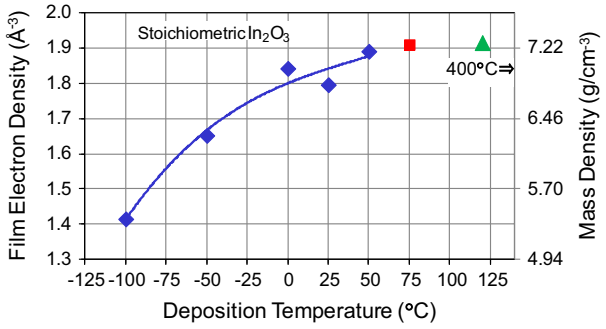

Fig. 3 Film electron density (left axis) of amorphous indium oxide films (blue diamonds) as a function of deposition temperature; film with first evidence of crystallinity deposited at 75 °C(red square) and fully crystalline film deposited at 400 °C (green triangle) included for comparison. Right axis: mass density assuming In_2O_3 stoichiometry.

systems such as quartz where α-quartz [30] has a density of 2.65 g/cm^3 and fused quartz [31] a density of 2.20 g/cm^3, a difference of ~19%.

3.3. *Effect of deposition temperature on electrical (Hall) properties*

The electrical properties of the films, as measured by Hall apparatus, are also dependent on deposition temperature. The carrier concentration, n, decreases with decreasing deposition temperature between +50 °C and −50 °C a difference of 32%, Fig. 4a; the film deposited at −100 °C was too resistive to measure. Care was taken to insure the oxygen partial pressure during deposition was kept constant between deposition temperatures as this can have a profound effect on carrier concentration. Any variation in oxygen partial pressure would be due to the precision of the pressure sensor and random. A portion of the decrease in carrier concentration can reasonably be attributed to the lessening of film density with decreasing deposition temperature; between +50 °C and −50 °C the film density decreased from 7.17 g/cm^3 to 6.27 g/cm^3, a difference of ~12%. To account for the additional decrease in carrier concentration two logical possibilities are; fewer carriers are generated (per unit mass) or traps that remove carriers are introduced as the deposition temperature is decreased. If fewer carriers are generated there should be fewer ionized oxygen vacancies and, at the high carrier concentrations present, the carrier mobility should increase with decreasing deposition temperature (carrier concentration) [14]. If carrier traps are generated then not only would the ionized oxygen vacancies scatter electrons but the charged carrier traps would also scatter electrons and the mobility should decrease with decreasing deposition temperature. This point will be revisited below in the discussion of carrier mobility. There is no sudden change in carrier concentration with the advent of crystallinity at +75 °C. For the highly crystalline film, there is a large decrease in carrier concentration: Highly crystalline IO frequently has low carrier concentration, hence the common practice of doping with tin to form ITO.

The carrier mobility, μ_H, decreases with decreasing temperature over the entire measurable amorphous range of +50 °C to −50 °C, Fig. 4b. As discussed above, this indicates the introduction of a scattering center in addition to the ones produced by ionized oxygen vacancies. Although this result supports to possibility of charged carrier traps, it is not possible to conclude the decrease in mobility is due to charged carrier traps; the decrease in mobility can also be due to structural imperfections that scatter the

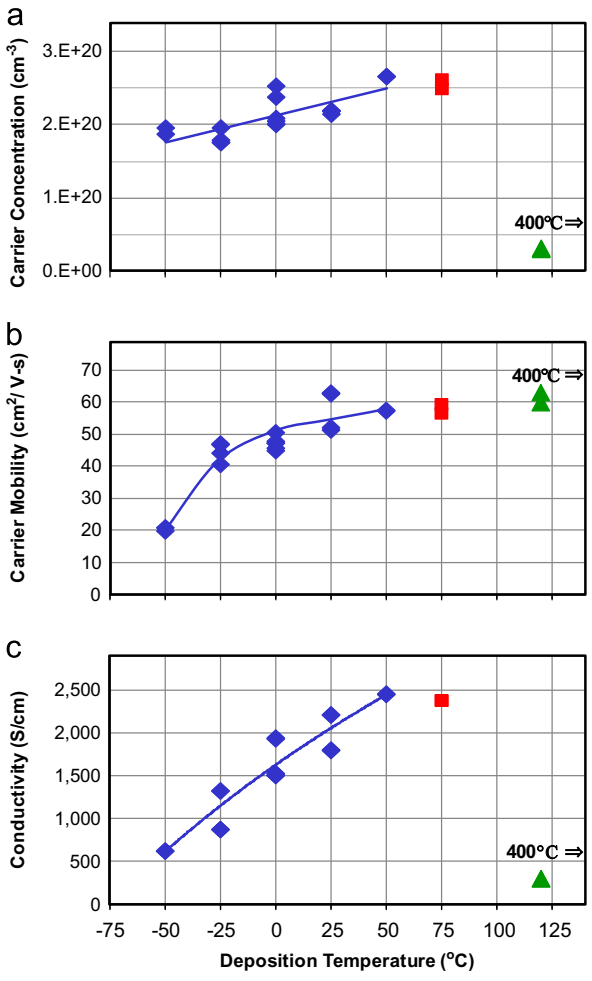

Fig. 4 Transport properties of amorphous indium oxide films (blue diamonds) as a function of deposition temperature; film with first evidence of crystallinity deposited at 75 °C(red square) and fully crystalline film deposited at 400 °C (green triangle) included for comparison.

electrons. This can be seen in crystalline IO and ITO where films with the same carrier density can have different carrier mobility depending on whether they are single-crystal like or poly-crystalline [13,14]; the nature of the structural imperfection in the amorphous material, however, may be different than those in the polycrystalline material. The conductivities, σ, Fig. 4c, are what would be expected given $\sigma = ne\mu$.

3.4. *Effect of deposition temperature on carrier scattering*

It is possible to calculate the effect on mobility due solely to ionized impurity centers [10,22] and subsequently separate the effects on mobility of carrier concentration and temperature-induced structural-change from each other. The effect of ionized impurity centers on mobility can be calculated from the expression:

$$\mu_I = [24\pi^3(\varepsilon_0\varepsilon_r)^2\hbar^3 n]/[e^3 m^{*2} g(x) Z^2 n_i], \quad (1)$$

where

$$g(x) = \ln(1+4/x) - 1/(1+x/4) \quad (2)$$

with

$$x = (4e^2 m^*)/[4\pi(\varepsilon_0\varepsilon_r)\hbar^2(3\pi^5)^{1/3} n^{1/3}] \quad (3)$$

In this set of equations μ_I is the carrier mobility one would observe if only ionized impurity centers were present, ε_o, $\hbar$, and e are the physical constants of the vacuum permittivity, Plank's constant and the electron charge, ε_r is the relative permittivity of indium oxide, m^* is the effective mass of a conduction electron, n the carrier density, Z is the charge of the ionized impurity center and n_i the density of ionized impurity centers. A relative permittivity of $\varepsilon_r = 9$ cited in the literature [14,32] will be used; the reported effective mass ranges between $0.28m_e$ and $0.43m_e$ [33–35] where m_e is the free electron mass, in this calculation $m^* = 0.3m_e$ will be used [26,28]; the carrier density, n, is obtained from Hall measurement; the ionized impurity centers will be assumed to be doubly-ionized oxygen vacancies [21,36,37], hence $Z = 2$; and that $n_i \approx n/Z$, hence $n_i = n/2$.

The easiest way to separate out the effect of ionized impurity centers from other sources of scattering is to look at scattering frequency, f, which is simply the inverse of the relaxation time,

$$f = 1/\tau. \quad (4)$$

Relation times add as an inverse sum,

$$1/\tau = \Sigma 1/\tau_i, \quad (5)$$

hence the total scattering frequency is the simple sum of the contributing scattering frequencies,

$$f = \Sigma f_i \quad (6)$$

The relaxation time is related to mobility by the expression

$$\mu = e\tau/m^* \quad (7)$$

hence

$$f = 1/\tau = e/\mu m^* \quad (8)$$

For any film, the total scattering frequency, f, can be determined from the measured Hall mobility, μ_H, and Eq. (8); the ionized scattering frequency, f_I, can be computed from the measured carrier concentration using Eqs. (1)–(3) and (8). Then the scattering frequency in excess of the ionized impurity scattering, f_{EX}, can be determined using Eq. (6).

$$f_{EX} = f - f_I \quad (9)$$

In this way the effect deposition temperature has on mobility can be examined independent of changes in carrier concentration in terms of f_{EX}.

The excess collision frequency as a function of deposition temperature is presented in Fig. 5. For a-IO films the excess collision frequency increase as the deposition temperature decreases, again this indicates the introduction of an additional scattering center. It has been proposed that mobility in IO based TCOs is proportional to the portion of edge-sharing InO_x polyhedral [38]; in the absence of edge-sharing polyhedral the scattering frequency increases and mobility decreases. Structural studies of IO by Utosuno et al. [39], reported a lower relative number of edge-sharing to corner-sharing InO_x polyhedral in a-IO than in c-IO. This would also increase the average In–In bond distance lowering the density of the film. For the films in this study, a decrease in the relative number of edge sharing InO_x polyhedral with deposition temperature would not only explain the decrease in film density with decreasing deposition temperature but also the increase in excess collision frequency (decrease in mobility). There is also no marked increase in scattering for the

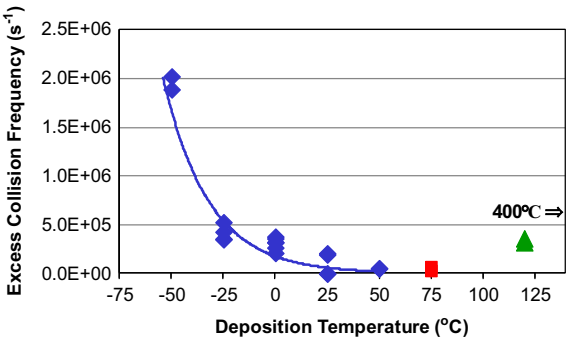

Fig. 5 Excess collision frequency of amorphous indium oxide films (blue diamonds) as a function of deposition temperature; film with first evidence of crystallinity deposited at 75 °C(red square) and fully crystalline film deposited at 400 °C (green triangle) included for comparison.

mixed a-IO/c-IO film deposited at +75 °C. The polycrystalline film deposited at 400 °C exhibits characteristics of having a scattering center in addition to those produced by ionized oxygen impurities. The analysis, however, is not strictly valid at the low carrier concentration of the sample (3×10^{19} cm^{-3}) where ionized oxygen impurity centers may not be the dominant scattering mechanism [24].

4. Conclusions

There are differences in both the physical and electrical properties of a-IO films beyond those that are commonly produced by the variation in oxygen content. One difference that is important to simulation studies is the film density. Our studies show that the film density is dependent on deposition temperature. The resulting differences in physical structure have an effect on the electrical properties of the films. For indium oxide and perhaps many of the indium oxide based systems, the best electrical properties of high mobility and high conductivity are observed for films grown at conditions close to those where crystallinity occurs.

Acknowledgements

For this research DBB and RPHC are supported by the U.S. Department of Energy, Office of Science, Office of Basic Energy Sciences under the Award Number DE-FG02-06ER46320: L.Z and M.J.B are supported by the MRSEC program of the National Science Foundation at Northwestern University under grant no. DMR-1121262. This work made use of; the J.B.Cohen x-ray Diffraction Facility supported by the MRSEC program of the National Science Foundation (DMR-1121262) at the Materials Research Center of Northwestern University; the Keck-II facilities of NUANCE supported by NSF-NSEC, NSF-MRSEC, Keck Foundation and the State of Illinois; the Optical Microscopy and Metallography Facility MRSEC program of the National Science Foundation.

References

[1] D.S. Ginley, C Bright, MRS Bulletin, Transparent conducting oxides, 25 (2000) 15–18.
[2] J.F. Wagner, D.A. Keszler, R.E. Presley, Transparent Electronics, Springer, New York, 2008.
[3] E. Fortunato, D. Ginley, H. Hosono, D.C. Paine, MRS Bulletin 32 (2007) 242–247.
[4] H. Hosono, Journal of Non-Crystalline Solids 352 (2006) 851–858.
[5] D.S. Ginley, H. Hosono, D.C. Paine (Eds.), Handbook of Transparent Conductors, Springer, New York, 2010.
[6] D.B. Buchholz, D.E. Proffit, M.D. Wisser, T.O. Mason, R.P.H. Chang, Progress in Natural Science: Materials International 22 (2012) 1–6.
[7] K. Nomura, H. Ohta, A. Takagi, T. Kamiya, M. Hirano, H. Hosono, Nature 432 (2004) 488–492.
[8] M. Ito, M. Kon, C. Miyazaki, N. Ikeda, M. Ishizaki, R. Matsubara, Y. Ugajin, N. Sekine, Physica Status Solidi A Applications and Material Science 205 (2008) 1885–1894.
[9] G.S. Chae, Japanese Journal of Applied Physics Part 1 (40) (2001) 1282–1286.
[10] M.P. Taylor, D.W. Readey, M.F.A.M. van Hest, C.W Teplin, J.L. Alleman, M.S. Dabney, L.M. Gedvilas, B.M. Keyes, B. To, J.D. Perkins, D.S. Ginley, Advanced Functional Materials 18 (2008) 3169–3178.
[11] W.M. Kim, D.Y. Ku, I.-K. Lee, Y.W. Seo, B.-K. Cheong, T.S. Lee, I.-H. Kim, K.S. Lee, Thin Solid Films 473 (2005) 315–320.
[12] M.K. Ryu, S. Yang, S.-H.K. Park, C.-S. Hwang, J.K. Jeong, Applied Physics Letters 95, 2009, 072104-1(3).
[13] D.Y. Lee, J.R. Lee, G.H. Lee, P.K. Song, Surface and Coating Technology 202 (2008) 5718–5723.
[14] J.R. Bellingham, W.A. Phillips, C.J. Adkins, Journal of Physics: Condensed Matter 2 (1990) 6207–6221.
[15] S.P. Harvey, T.O. Mason, D.B. Buchholz, R.P.H. Chang, Journal of the American Ceramic Society 91 (2008) 467–472.
[16] D.B. Buchholz, J. Liu, T.J. Marks, M. Zhang, R.P.H. Chang, ACS Applied Materials & Interfaces 1 (2009) 2147–2153.
[17] A.K. Kulkarnia, K.H. Schulzb, T.S. Lima, M. Khanb, Thin Solid Films 345 (1999) 273–277.
[18] R.B.H. Tahar, T. Ban, Y. Ohya, Y. Takahashi, Journal of Applied Physics 83 (1998) 2631–2645.
[19] A.J. Freeman, K.R. Poppelmeier, T.O. Mason, R.P.H. Chang, T.J. Marks, MRS Bulletin (2000) 45–51 (August).
[20] T. Minami, Journal of Vacuum Science and Technology A 17 (1999) 1765–1772.
[21] P.K. Song, H. Akao, M. Kamei, Y. Shigesato, I. Yasui, Japanese Journal of Applied Physics Part 1 38 (1999) 5224–5226.
[22] H. Nakazawa, Y. Ito, E. Matsumoto, K. Adachi, N. Aoki, Y. Ochiai, Journal of Applied Physics 100 (2006) (093706-1(7).
[23] R.B. Dingle, Philosophical Magazine 46 (1955) 831–840.
[24] K. Makise, B. Shinozaki, T. Asano, K. Mitsuishi, K. Yano, K. Inoue, H. Nakamura, Journal of Applied Physics 112 (2012) (033716-1(6).
[25] A second difference might have been film thickness, However the film thicknesses in the studies were 150 nm and 200 nm respectively; too small a difference to account for such a large difference in mobility.
[26] J. Rosen, O. Worschkow, Physical Review B: Condensed Matter 80 (2009) (115215-1(10).
[27] A. Nelson, Journal of Applied Crystallography 39 (2006) 273–276.
[28] F.O. Adurodija, L. Semple, R. Brüning, Journal of Material Science 41 (2006) 7096–7102.
[29] H. Swenson, et al., National Bureau of Standards (US), Circular 539 (5), 26 (1955) (PDF 00-006-0416).
[30] ⟨http://www.mindat.org/min-3337.htm⟩.
[31] ⟨http://www.quartz.com/gedata.html#table⟩.
[32] I. Hamberg, C.G. Granqvist, Journal of Applied Physics 60 (1986) R123–R159.
[33] Y. Ohhata, F. Shinoki, S. Yoshida, Thin Solid Films 59 (1979) 255–261.
[34] R. Clanget, Applied Physics 2 (1973) 247–256.

[35] H. Köstlin, R. Jost, W. Lems, Physica Status Solidi A Applications and Material Science 29 (1975) 87–93.
[36] Y. Shigesato, D.C. Paine, Applied Physics Letters 62 (1992) 1268–1270.
[37] B.J. Ingram, G.B. Gonzalez, D.R. Kammer, M.I. Bertoni, T.O. Mason, Journal of Electroceramics 13 (2004) 167–175.
[38] T. Kamiya, K. Nomura, H. Hosono, Journal of display Technology 5 (2009) 273–288.
[39] F. Utsuno, H. Inoue, I. Yasui, Y. Shimane, S. Tomai, S. Matsuzaki, K. Inoue, I. Hirosawa, M. Sato, T. Honma, Thin Solid Films 496 (2006) 95–98.